



Published in final edited form as:

Neuron. 2020 August 05; 107(3): 580–589.e6. doi:10.1016/j.neuron.2020.05.007.

Plasticity and spontaneous activity pulses in disused human brain circuits

Dillan J. Newbold^{1,17,*}, Timothy O. Laumann², Catherine R. Hoyt³, Jacqueline M. Hampton², David F. Montez^{1,2}, Ryan V. Raut⁴, Mario Ortega¹, Anish Mitra^{4,5}, Ashley N. Nielsen^{1,6}, Derek B. Miller¹, Babatunde Adeyemo¹, Annie L. Nguyen¹, Kristen M. Scheidter¹, Aaron B. Tanenbaum¹, Andrew N. Van^{1,7}, Scott Marek¹, Bradley L. Schlaggar^{1,8,9,10}, Alexandre R. Carter^{1,3}, Deanna J. Greene^{2,4}, Evan M. Gordon^{11,12,13}, Marcus E. Raichle^{1,4}, Steven E. Petersen^{1,4,7,14,15}, Abraham Z. Snyder^{1,4}, Nico U.F. Dosenbach^{1,3,4,7,16,*}

¹Department of Neurology, Washington University School of Medicine, St. Louis, MO 63110, USA.

²Department of Psychiatry, Washington University School of Medicine, St. Louis, MO 63110, USA.

³Program in Occupational Therapy, Washington University School of Medicine, St. Louis, MO 63110, USA.

⁴Department of Radiology, Washington University School of Medicine, St. Louis, MO 63110, USA.

⁵Department of Psychiatry, Stanford University, Stanford, CA 94305, USA.

⁶Institute for Innovations in Developmental Sciences, Northwestern University, Chicago, IL 60611, USA.

⁷Department of Biomedical Engineering, Washington University in St. Louis, St. Louis, MO 63110, USA.

⁸Kennedy Krieger Institute, Baltimore, MD 21205, USA.

⁹Department of Neurology, Johns Hopkins University School of Medicine, Baltimore, MD 21287, USA.

¹⁰Department of Pediatrics, Johns Hopkins University School of Medicine, Baltimore, MD 21287, USA.

¹¹VISN 17 Center of Excellence for Research on Returning War Veterans, Waco, TX 76711, USA.

*Correspondence: newbold@wustl.edu, dosenbachn@wustl.edu.

Author Contributions:

D.J.N., T.O.L., C.R.H., A.Z.S., and N.U.F.D. designed the study. A.N.N. and N.U.F.D. volunteered as participants. D.J.N., C.R.H., J.M.H., and K.M.S. collected the behavioral data. D.J.N., J.M.H., M.O., A.L.N., K.M.S., and N.U.F.D. collected the MRI data. D.J.N., T.O.L., C.R.H., D.F.M., M.O., D.B.M., B.A., A.B.T., A.N.V., E.M.G. and A.Z.S. analyzed the data. D.J.N., T.O.L., C.R.H., D.F.M., R.V.R., M.O., A.M., A.N.N., B.A., S.M., B.L.S., A.R.C., D.J.G., E.M.G., M.E.R., S.E.P., A.Z.S., and N.U.F.D. interpreted the results. D.J.N., T.O.L., M.E.R., A.Z.S., and N.U.F.D. wrote the manuscript with input from all other authors.

Declaration of interests:

The authors declare the following competing financial interest: N.U.F.D. is co-founder of NOUS Imaging.

Publisher's Disclaimer: This is a PDF file of an unedited manuscript that has been accepted for publication. As a service to our customers we are providing this early version of the manuscript. The manuscript will undergo copyediting, typesetting, and review of the resulting proof before it is published in its final form. Please note that during the production process errors may be discovered which could affect the content, and all legal disclaimers that apply to the journal pertain.

¹²Center for Vital Longevity, School of Behavioral and Brain Sciences, University of Texas at Dallas, Dallas, TX 75080, USA.

¹³Department of Psychology and Neuroscience, Baylor University, Waco, TX 76706, USA.

¹⁴Department of Neuroscience, Washington University School of Medicine, St. Louis, MO 63110, USA.

¹⁵Department of Psychological and Brain Sciences, Washington University in St. Louis, St. Louis, MO 63110, USA.

¹⁶Department of Pediatrics, Washington University School of Medicine, St. Louis, MO 63110, USA.

¹⁷Lead Contact

SUMMARY

To induce brain plasticity in humans, we casted the dominant upper extremity for two weeks and tracked changes in functional connectivity using daily 30-minute scans of resting-state functional MRI (rs-fMRI). Casting caused cortical and cerebellar regions controlling the disused extremity to functionally disconnect from the rest of the somatomotor system, while internal connectivity within the disused sub-circuit was maintained. Functional disconnection was evident within 48 hours, progressed throughout the cast period, and reversed after cast removal. During the cast period, large, spontaneous pulses of activity propagated through the disused somatomotor sub-circuit. The adult brain seems to rely on regular use to maintain its functional architecture. Disuse-driven spontaneous activity pulses may help preserve functionally disconnected sub-circuits.

In brief

Newbold *et al.* induced human brain plasticity by casting the dominant arm for two weeks. Disused brain regions rapidly (<48 hours) disconnected from the motor system and manifested large spontaneous activity pulses. Maintaining the brain's functional architecture may require regular use, and spontaneous activity pulses could serve as a substitute.

INTRODUCTION

Use-driven plasticity is critical for shaping neural circuits during development, learning, and recovery from injury (Murphy and Corbett, 2009; Reynolds et al., 2001; Wiesel and Hubel, 1965). Yet, the large-scale functional organization of the human brain is remarkably stable from day to day and largely robust to changes in behavioral state (Gratton et al., 2018; Laumann et al., 2015). Resting-state functional magnetic resonance imaging (rs-fMRI) provides a powerful means of examining human brain organization by recording spontaneous neural activity, i.e., activity not related to external stimuli or overt behaviors. Spontaneous activity consumes the vast majority of the brain's metabolic energy (Raichle, 2006) and is synchronized within functionally related regions, a phenomenon known as functional connectivity (FC) (Biswal et al., 1995). FC is characteristically strong between corresponding regions of the left and right hemispheres (homotopic regions) and within

large-scale functional systems with distinct cognitive functions (Power et al., 2011; Yeo et al., 2011).

It has been hypothesized that FC is modulated through Hebbian-like processes, such that FC is strengthened through coactivation of brain regions (Dosenbach et al., 2008; Guerra-Carrillo et al., 2014; Harmelech and Malach, 2013; Lewis et al., 2009; Shannon et al., 2016). Previous attempts to induce changes in brain organization using training paradigms have shown only subtle changes in FC ($r \sim 0.1$) (Guerra-Carrillo et al., 2014; Harmelech and Malach, 2013; Lewis et al., 2009; Shannon et al., 2016). In addition, prior studies relied on endpoint measurements and were therefore unable to describe the time courses of FC alterations. Developmental FC changes (Dosenbach et al., 2010; Grayson and Fair, 2017; Nielsen et al., 2019; Smyser et al., 2010) suggest that patterns of coactivation could be accumulated over years, but little is known about the effects of behavioral changes on brain organization over shorter time frames.

To induce FC changes in human participants, we adopted an approach used in classic animal plasticity studies, which impose sensory or motor deprivation (e.g., monocular deprivation, deafferentation, limb constraint) in a small number of intensively studied individuals (Merzenich et al., 1983; Milliken et al., 2013; Wiesel and Hubel, 1965). We casted the dominant upper extremity of three adult participants ('Nico', 'Ashley' and 'Omar') for two weeks and tracked changes in FC over 6–9 weeks using daily 30-minute rs-fMRI scans (21–32 hours of rs-fMRI/participant, 152 scans total; Figures 1A and S1). This highly sampled, longitudinal approach allowed us to measure disuse-driven plasticity in each individual and replicate results across all participants.

RESULTS

Casting caused disuse and reduced strength of the dominant upper extremity

Casts constrained movement of the elbow, wrist and fingers (Figure 1B). Accelerometers worn continuously on both wrists documented greatly reduced use of the casted upper extremity (Figures 1C and S1; use counts; Nico: –41%, Ashley: –55%, Omar: –46%). Immediately after cast removal, participants showed reduced grip strength (Figure 1D; dynamometry; Nico: –27%, Ashley: –42%, Omar: –39%) and reduced fine motor skill (Figure S1; Purdue Pegboard; Nico: –24%, Ashley: –29%, Omar: –12%). Participants showed increased use of the un-casted upper extremity (Figure S1; Nico: +24%, Ashley: +15%, Omar: +23%) and reported subjective improvement in the use of this extremity during activities of daily living (Video S1), but they did not consistently show improvements in strength or fine motor skill (Figures 1D and S1).

Disused somatomotor regions became functionally uncoupled from remainder of the somatomotor system

FC was originally discovered by Biswal *et al.* between the right upper-extremity primary somatomotor cortex (L-SM1_{ue}) and the homotopic region of the opposite hemisphere (R-SM1_{ue}) (Biswal et al., 1995). Prior to casting, all participants showed strong homotopic FC between L-SM1_{ue} and R-SM1_{ue} (Figures 2A and 2B). Casting led to a large reduction in FC

between L-SM1_{ue} and R-SM1_{ue} in all participants (Figure 2B; Nico: $r = -0.23$, Ashley: $r = -0.86$, Omar: $r = -0.61$). We also found significantly decreased FC between the disused upper-extremity region of the cerebellum (R-Cblm_{ue}) and its homotopic counterpart (L-Cblm_{ue}; Figure S2; Nico: $r = -0.16$, Ashley: $r = -0.07$, Omar: $r = -0.33$). Decreased homotopic FC was somatotopically specific to the disused upper-extremity somatomotor cortex and cerebellum (L-SM1_{ue}:R-SM1_{ue}, R-Cblm_{ue}:L-Cblm_{ue}) and did not occur in lower-extremity (L-SM1_{le}:R-SM1_{le}, R-Cblm_{le}:L-Cblm_{le}) or face regions (L-SM1_{face}:R-SM1_{face}, R-Cblm_{face}:L-Cblm_{face}; Figures 2C, 2D and S2). In all participants, FC decreases became significant within 48 hours of casting (Nico: Cast day 2 $r = -0.22$, $P < 0.001$; Ashley: Cast day 1 $r = -0.23$, $P < 0.001$; Omar: Cast day 1 $r = -0.83$, $P < 0.001$). While disused regions in the somatomotor cortex and cerebellum (L-SM1_{ue} and R-Cblm_{ue}) were functionally disconnected from the opposite hemisphere, these same regions became more connected to each other (Figures S2). The net effect was that disused brain regions dissociated from the remainder of the somatomotor system (Figure 3). All effects returned to baseline within days after cast removal (Figures 2, 3 and S2).

Spontaneous activity pulses emerged in the disused somatomotor cortex during casting

To further characterize the changes in spontaneous activity caused by casting, we closely examined rs-fMRI signals in L-SM1_{ue} and R-SM1_{ue}. During the cast period, all participants showed significantly increased amplitude of low-frequency fluctuations (ALFF) in L-SM1_{ue} (Figure 4A; Nico: +22%, Ashley: +81%, Omar: +36%) and one participant showed increased ALFF in R-SM1_{ue} (Figure 4B; Ashley: +26%). Increased ALFF was specific to the upper-extremity somatomotor cortex and did not occur in adjacent regions (L-SM1_{le} and L-SM1_{face}; Figures 4C and 4D). Unexpectedly, inspection of the rs-fMRI timeseries revealed large, spontaneous pulses of activity during the cast period (Figures 5A and S3). We termed these events “disuse pulses”. The shape of disuse pulses (Figures 5B and S3) resembled the canonical hemodynamic response to a brief stimulus (Lindquist et al., 2009). Disuse pulses had a large amplitude (up to 1.5% signal change) and were easily distinguished from ongoing spontaneous fluctuations in L-SM1_{ue} (<0.5% signal change; Figures 5A and S3). Pulses were essentially absent prior to casting (Nico: 1.1 pulses/scan; Ashley: 0.2; Omar: 1.0), occurred frequently during the cast period (Nico: 4.2; Ashley: 11.4; Omar: 12.3), and were infrequent after cast removal (Nico: 0.9; Ashley: 0.8; Omar: 1.9; Figure 5C).

Disuse pulses propagated through the disused somatomotor sub-circuit

Disuse pulses were not only present in L-SM1_{ue} but propagated throughout the disused upper-extremity sub-circuit, i.e., L-SM1_{ue}, L-SMA_{ue}, and R-Cblm_{ue} (Figures 6A and S4). A consistent pattern of pulse propagation was observed in all participants. Pulses sequentially occurred in L-SMA_{ue}, L-SM1_{ue} and then R-Cblm_{ue}, with mean time delays of ~200ms and ~600ms, respectively (Figures 6B, 6C and S4). This sequence of temporal lags is similar to that found in ongoing spontaneous activity (Marek et al., 2018; Mitra et al., 2014; Nielsen et al., 2019; Raut et al., 2020). Monitoring of upper extremity movements in one participant (Omar), using a highly sensitive pressure bladder placed inside the cast, showed that most pulses occurred in the absence of movements (Figure S5). To verify that spontaneous activity changes observed during the cast period were due to disuse during daily life rather

than the presence of casts during scanning, we conducted a control experiment in which participants wore removable casts only during 30-minute scans. We found only minimal changes in FC and almost no pulse-like events, indicating that the large decreases in FC and numerous disuse pulses observed during the cast period were not driven by wearing a cast during scans (Figure S6).

DISCUSSION

Disuse drives large decreases in functional connectivity

The magnitude of FC changes induced by casting ($r = -0.23, -0.86, -0.61$) is noteworthy because FC is typically highly stable from day to day (Gratton et al., 2018; Laumann et al., 2015). By the end of the two-week cast period, FC in all participants was as low as has been observed after motor stroke (Carter et al., 2012) or limb amputation (Makin et al., 2013). Animal studies that pharmacogenetically manipulated specific brain regions were able to drive large changes in FC ($r > 0.3$) (Grayson et al., 2016; Rosenthal et al., 2019). Yet, prior human studies of experimentally induced plasticity found much smaller effects ($r \sim 0.1$) (Guerra-Carrillo et al., 2014; Lewis et al., 2009; Shannon et al., 2016). Key differences between the current experiment and previous studies are: 1) use of a sustained behavioral intervention, 2) inducing disuse as opposed to training a skill, 3) measuring daily time courses (Wenger et al., 2017) rather than comparing only pre/post, 4) overcoming sampling variable with longer (30-minute) scans (Gordon et al., 2017; Laumann et al., 2015), and 5) conducting analyses at the level of individual participants, enabling three-fold replication of all major findings.

Functional connectivity can change rapidly over a span of days

The observed loss of homotopic FC during disuse, corroborated by animal models of visual deprivation and deafferentation (Kraft et al., 2017; Pawela et al., 2010), supports the hypothesis that FC can be strengthened by coactivation of brain regions (Guerra-Carrillo et al., 2014; Harmelech and Malach, 2013; Lewis et al., 2009; Shannon et al., 2016). The interval over which the effects of coactivation are accumulated was previously unknown (Guerra-Carrillo et al., 2014; Harmelech and Malach, 2013; Lewis et al., 2009). Some have suggested that patterns of coactivation are accumulated over many years (Shannon et al., 2016). However, the current results demonstrate that FC can be significantly altered within 12–48 hours when a sufficiently strong behavioral constraint is imposed, suggesting that FC is determined, at least in part, by a person's recent behaviors and experiences. The close relationship between FC and recent behavior raises the fascinating possibility that group differences in FC found in certain neuropsychiatric conditions, e.g., stroke (Carter et al., 2012; Siegel et al., 2018), Parkinson's disease (Gratton et al., 2019), Tourette syndrome (Nielsen et al., 2020) and limb amputation (Makin et al., 2013), may in part reflect disease-specific differences in day-to-day behavior.

Disused sub-circuits maintain internal connectivity

In addition to disconnecting from the opposite hemisphere, disused regions (L-SM1_{ue} and R-Cblm_{ue}) became more strongly connected to each other. Increased FC amongst disused regions has also been observed in mice during binocular deprivation (Kraft et al., 2017).

Disuse-driven increases in FC were not predicted by the Hebbian FC hypothesis. A straightforward Hebbian account would have predicted that disused regions should disconnect from all other regions. Rather, FC amongst disused regions (L-SM1_{ue} and R-Cblm_{ue}) seems to have increased due to synchronized pulses of activity during the cast period.

Spontaneous activity shapes neural circuits during development

The presence of spontaneous pulses in the disused somatomotor sub-circuit may reflect processes that help maintain the functional organization of the adult brain. Simultaneously, pulses may also have contributed to reductions in FC between the disused sub-circuit and the remainder of the somatomotor system. Spontaneous activity serves several known roles in shaping neural circuits (Buzsáki, 2019). Hippocampal sharp-wave ripples and thalamic sleep spindles are thought to facilitate transfer of newly formed memories to the cortex (Buzsaki, 2015; Klinzing et al., 2019). Moreover, large-amplitude transients at low frequencies, similar to the disuse pulses described here, are a hallmark feature of developing brains and help to shape brain-wide circuits *in utero* (Tolonen et al., 2007). In the developing visual system, spontaneous waves of activity originate in the retina and propagate through the entire visual system, helping to link circuits across several cortical and subcortical regions (Ackman et al., 2012; Katz and Shatz, 1996). Similar activity-dependent refinement of the somatomotor system is triggered by spontaneous activation of spinal motor neurons (Khazipov et al., 2004). The finding of disuse pulses in our participants suggests that adult brain circuits may retain a latent potential to self-organize through spontaneous activity. Spontaneous activity transients seen in development show a characteristic pattern of electrical activity, known as delta-brushes (Khazipov et al., 2004; Tolonen et al., 2007). Future experiments utilizing electroencephalography (EEG) in humans or microelectrode recording in animals will allow closer comparison of disuse pulses to spontaneous activity transients.

Focal disinhibition may allow for the emergence of spontaneous activity pulses

The disuse pulses observed in our participants were larger (up to 1.5% signal change) than the spontaneous activity fluctuations typically observed in the adult brain and may have resulted from disinhibition of disused circuits. During postnatal critical periods, inhibitory interneurons begin to suppress spontaneous activity, shifting the primary driver of activity-dependent plasticity from internal to external sources (Toyoizumi et al., 2013). Perhaps as a result of increased inhibitory tone, spontaneous activity in the adult brain does not typically include transients and is instead characterized by ongoing, stationary fluctuations (Laumann et al., 2017). Disused circuits exhibit characteristic changes in local physiology: principal cells begin responding to previously silent inputs (Merzenich et al., 1983; Wiesel and Hubel, 1965), inhibitory interneurons become less active (Gainey et al., 2018), and the synapses between inhibitory interneurons and principal cells are weakened (Wellman et al., 2002). Disuse-driven disinhibition may permit the reemergence of spontaneous pulses of activity in the adult brain. Indeed, pharmacogenetic suppression of inhibitory interneurons in the somatosensory cortex of adult mice produces spontaneous bursts of activity that propagate to functionally connected regions (Rosenthal et al., 2019). Focal disinhibition is also thought to occur after stroke (Liepert et al., 2000), another condition in which circuits are disused (van

der Pas et al., 2011). An important question is whether disuse pulses arise during stroke recovery and how they impact clinical outcomes.

The human brain – plastic yet stable

In the absence of regular use, our participants showed rapid loss of homotopic somatomotor FC. Thus, the human brain retains a surprising capacity for use-driven plasticity into adulthood. Simultaneously, large pulses of spontaneous activity began propagating through the disused somatomotor sub-circuit, helping to maintain its internal functional connectivity. Since somatomotor connectivity and motor performance returned to baseline quickly after cast removal, disuse pulses may have protected the integrity of the disused sub-circuit. Functional disconnection of disused sub-circuits, stabilized by spontaneous activity pulses, may allow the brain to reorganize itself rapidly without compromising its overall stability. Disuse pulses, analogous to waves of spontaneous activity seen during development, may allow the adult brain to bridge the seeming chasm between plasticity and stability.

STAR METHODS

RESOURCE AVAILABILITY

Lead Contact—Further information and requests for resources and reagents should be directed to and will be fulfilled by the Lead Contact, Dillan Newbold (newbold@wustl.edu).

Materials Availability—This study did not generate new unique reagents.

Data and code availability—The neuroimaging data generated during this study are available on OpenNeuro (www.openneuro.org/datasets/ds002766). All code needed to reproduce our analyses is available on Gitlab (<https://gitlab.com/DosenbachGreene/cast-induced-plasticity>).

EXPERIMENTAL MODEL AND SUBJECT DETAILS

Human participants—Participants were three healthy, adult volunteers. All denied recent injuries of the dominant upper extremity and any contraindications to MRI (e.g., metallic implants, claustrophobia). Because of the large amount of data collected, we were able to analyze each participant individually, allowing us to test all hypotheses in triplicate. The first participant was a 35-year-old male who was a participant in the Midnight Scan Club experiment (MSC02) (Gordon et al., 2017; Greene et al., 2020; Marek et al., 2018; Sylvester et al., 2020) and the senior investigator of this study (N.U.F.D., ‘Nico’). The second participant was a 25-year-old female, also drawn from the Midnight Scan Club cohort (MSC06) and was a member of the research team (A.N.N., ‘Ashley’). The third participant was a 27-year-old male (‘Omar’). All participants were right handed, as assessed by the Edinburgh Handedness Inventory (Oldfield, 1971) (Nico: +100, right-handed; Ashley: +91, right-handed; Omar: +60, right-handed). The Washington University School of Medicine Institutional Review Board approved the study protocol and provided experimental oversight. Participants provided informed consent for all aspects of the study and were paid for their participation. Participants also consented to be identified in publications, presentations and media releases by inclusion of their photographs and names.

METHODS DETAILS

Experimental intervention—Constraint of the dominant upper extremity was achieved by fitting each participant with a fiberglass cast that extended from just below the shoulder to past the fingertips. Casts contained an inner layer of Delta-Dry water-resistant padding (BSN Medical, Luxembourg) that provided a comfortable layer of cushioning permitting airflow; thus, participants could bathe without developing skin irritation. Extra padding was applied around the ulnar styloid process, olecranon and antecubital fossa. A strong outer shell was constructed from Delta-Lite Plus fiberglass casting tape. Tape was applied with the elbow bent at a natural angle (approximately 95°), the wrist slightly extended, the fingers slightly flexed, and the thumb extended. Casts were constructed by an Occupational Therapist (C.R.H.) specially trained in therapy involving casting. All participants were fit with a temporary cast several days before the two-week casting period to practice achieving a comfortable position; practice casts were removed after about 10 minutes. In one participant (Omar), the cast was remade after one day to correct uncomfortable finger position. All casts were removed using a specialized, oscillating blade saw that cuts fiberglass without harming the underlying skin.

In order to test for any effects of wearing casts during scans, we cut the casts from the original experiment in half along their long axes, applied felt to the inside surfaces and all cut edges, and added Velcro fasteners to create casts that could be easily applied and removed at the start and end of scanning. Participants wore removable casts during half of the rs-fMRI sessions acquired during a control experiment but did not wear these casts during daily activities.

Activity monitoring—Behavior during normal daily life was assessed using accelerometers worn on each wrist. All participants wore a wGT3X-BT accelerometer (Actigraph, Pensacola) on each wrist throughout the day and night for the full duration of the experiment. The only times participants removed their accelerometers were during daily MRI scans. The accelerometers recorded acceleration along three orthogonal dimensions with a sampling rate of 30Hz.

Strength testing—Grip strength was measured with a Jamar Smart Hand Digital Dynamometer (Patterson Medical, Warrenton). Participants were instructed to form a closed fist around a handle on the dynamometer, keeping the arm at the side with the elbow bent at 90°, and squeeze as tightly as possible. Maximal force was recorded in pounds. This was repeated for each hand in triplicate at each measurement time point (Figure 1D).

Fine motor testing—Fine motor function of each upper extremity was assessed using the Purdue pegboard task (Tiffin and Asher, 1948). Participants were instructed to use one hand to pick up small (~1 inch) metal pegs one at a time from a bin and insert them into a row of small holes on a pegboard. Participants were given 30 seconds to insert as many pegs as possible. The task was then repeated with the other hand. This task was repeated in triplicate at each assessment (Figure S1C).

MRI acquisition—Participants were scanned every day of the experiment, for 42–64 consecutive days, except for rare days when the scanner or the participant was unavailable (Figure S1). Imaging was performed at a consistent hour of the day (Supplementary Table 1) to minimize diurnal effects in functional connectivity (Shannon et al., 2013). Sequence details are listed in Supplementary Table 1. Every session included a 30-minute resting-state blood oxygen level-dependent (BOLD) fMRI scan, during which participants were instructed to hold still and look at a white fixation crosshair presented on a black background. During one scan (Ashley, scan 21), the fixation crosshair was not presented until 5 minutes into the scan, so these 5 minutes of data were excluded from further processing. Head motion was tracked in real time using Framewise Integrated Real-time MRI Monitoring software (FIRMM) (Dosenbach et al., 2017). An eye-tracking camera (EyeLink, Ottawa) was used to monitor participants for drowsiness. Some sessions prior to casting (Figure S1) included motor tasks, during which participants were instructed to move their left hand, right hand, left foot, right foot, or tongue in a block design cued by visual stimuli (Barch et al., 2013). Two 4-minute runs of this task were completed during each task session.

Hand movement monitoring—Hand movements during rs-fMRI scans were tracked using a highly sensitive pneumatic bladder (Siemens, Munich), originally designed for tracking respiratory movements. This bladder was inserted into the end of the cast, along the palmar surface of the fingers during rs-fMRI scans (see Figure S5 for a photo showing the bladder position). Instructing the participant to make very small hand movements during a test run confirmed that the bladder was extremely sensitive to movements at the finger joints, wrist, elbow and shoulder. Additionally, although the bladder was inserted inside the cast, we were still able to detect respiration.

QUANTIFICATION AND STATISTICAL ANALYSIS

Analysis of accelerometry data—Data from wrist-based accelerometers were transferred off of the devices during MRI scans and down sampled to 1Hz. All analyses were based on a root mean square (RMS) of the three acceleration directions. Use counts were calculated as the number of seconds per day when the RMS acceleration exceeded a noise threshold of 10 accelerometer units (Hoyt et al., 2019) (1 accelerometer unit = 0.016 m/s²). Periods of sleep were detected as blocks of 15 minutes or more with a use count below 100. “% Time Moving” reported in Figure S1B was calculated as the daily use count normalized by the total number of waking seconds recorded each day. Use ratios reported in Figure 1C were calculated as the ratio of use counts for the left and right upper extremities.

MR image processing—Structural images (T1- and T2-weighted) were corrected for gain field inhomogeneity using FSL Fast (Zhang et al., 2001), and aligned to the 711–2B implementation of Talairach atlas space using the 4dfp MRI processing software package (<https://readthedocs.org/projects/4dfp/>). The 711–2B template conforms to the 1988 Talairach atlas (Talairach and Tournoux, 1988) according to the method of Lancaster *et al.* (Lancaster et al., 1995). Relative to MNI152, 711–2B space is about 5% smaller and 2° anteriorly rotated about the ear-to-ear axis. Mean T1- and T2-weighted images (T1w and T2w) were computed by coregistration and averaging multiple acquisitions. The mean T1w

for each participant was run through the FreeSurfer pipeline (version 5.3) (Fischl, 2012) to generate an anatomical segmentation and 3D surface models of the cerebral cortex.

fMRI processing followed a previously published pipeline (Raut et al., 2019). Briefly, preprocessing included temporal interpolation to correct for slice time differences, correction of intensity differences between odd and even slices and rigid-body correction for head movement. Atlas transformation of the functional data was computed as a composition of transforms: native space mean functional image \rightarrow T2w \rightarrow T1w \rightarrow atlas representative template. The functional data were resampled in atlas space in one step including correction for susceptibility inhomogeneity-related distortion (Jenkinson et al., 2012).

Denosing was accomplished by regression of nuisance time series following a CompCor-like strategy (Behzadi et al., 2007; Raut et al., 2019). Regressors included the 6 rigid parameters derived by retrospective motion correction, the global signal averaged over the brain, and orthogonalized waveforms extracted from the ventricles, white matter and extracranial tissues (excluding the eyes). Frame censoring (scrubbing) was computed on the basis of both frame-wise displacement (FD) and variance of derivatives (DVARS) measures (Power et al., 2012) with thresholds set individually for each participant (Supplementary Table 1). Rigid-body motion parameters were low-pass filtered (< 0.1 Hz) prior to FD computation to remove respiratory artifacts in head-motion estimates (Fair et al., 2020). Grayordinate image intensity plots (Power, 2017) were visually checked to confirm artifact reduction. The data then were temporally bandpass filtered prior to nuisance regression, retaining frequencies between 0.005 Hz and 0.1 Hz. Censored frames were replaced by linearly interpolated values prior to filtering and re-censored afterwards.

Preprocessed functional data (BOLD time series) were extracted from the cerebral cortex and cerebellum using FreeSurfer-based segmentations and cortical surface models. Cortical data were projected onto a 2D surface (generated by FreeSurfer) using tools distributed as part of the Human Connectome Workbench software package (Marcus et al., 2011). As previously described (Gordon et al., 2017), cortical projection involves selecting voxels that fall between two surface models fit to the inner and outer surfaces of the cortex and interpolating between these voxels to project BOLD data from each cortical hemisphere to a $\sim 164,000$ -vertex 2D surface. Surface projected data are then downsampled to $\sim 32,000$ -vertices and geodesically smoothed using a 2-dimensional 6-mm full-width half max (FWHM) smoothing kernel. Cerebellar voxels were kept in volume space and smoothed using a 3-dimensional 4.7mm FWHM kernel.

ROI selection—Most analyses utilized individual-specific task-defined regions of interest (ROIs). Task-defined ROIs were selected using an automated analysis of task fMRI data, as previously described (Marek et al., 2018). For each movement in the motor task (hand, tongue or foot movement), we selected ROIs inside of two anatomical regions, which were automatically labeled by FreeSurfer: the primary somatomotor cortex (pre- and post-central gyri) and the superior half of the cerebellum. To select ROIs within each anatomical region, we first located the vertex/voxel showing maximal task synchrony (Marek et al., 2018) during the motor task and then grew the ROI to a preset size (400 vertices in the somatomotor cortex, 40 voxels in the cerebellum) by selecting neighboring vertices/voxels

in descending order of task synchrony. ROIs for an example participant (Omar) are shown in Figure 2.

The graph-theoretic analyses shown in Figure 3 required multiple ROIs per somatomotor region in order to showcase connectivity both within and between regions. To select ROIs for graph analyses, a set of parcels spanning the entire cerebral cortex was generated for each participant, and each parcel was assigned to one of 17 canonical functional networks using a graph theory-based community detection algorithm (Rosvall and Bergstrom, 2008). Parcels and network assignments for our first two participants (Nico and Ashley) were previously generated and published (Gordon et al., 2017). We used identical methods for our third participant (Omar).

Functional connectivity measurement—Mean BOLD time series were extracted from each ROI by averaging the time series of all vertices within the ROI. Functional connectivity between ROIs was then measured for each session by computing the Pearson correlation between mean ROI BOLD time series, excluding high-motion frames (Supplementary Table 1). Daily time series of functional connectivity between ROIs are shown in Figure 2. Functional connectivity seed maps were computed for the left-hemisphere somatomotor cortex (L-SM1_{UE}) ROI for each session by correlating the mean time series from the ROI with the time series from every voxel. Seed maps are shown in Figure 2.

Exponential decay model—The daily time course of functional connectivity between regions of interest (ROIs) was modeled using the following differential equation:

$$\frac{dr}{dt} = \alpha(r_{\infty} - r) \quad (1)$$

$$r_{\infty} = \begin{cases} r_c & \text{if casted} \\ r_0 & \text{if not casted} \end{cases} \quad \alpha = \begin{cases} \alpha_1 & \text{during casting} \\ \alpha_2 & \text{after casting} \end{cases}$$

where r is the current functional connectivity between two ROIs, r_0 is the baseline functional connectivity, r_c is the equilibrium functional connectivity in the casted state, α_1 describes the rate of change during the cast period and α_2 describes the rate of change during the post period. r_0 was set to the mean functional connectivity in the pre period. The other three parameters (r_c , α_1 and α_2) were fit to the data using a least squares approach.

Total change in functional connectivity (Δr) reported in Figures 2 and S2, was computed as the difference between the modeled functional connectivity (r) at the end of the cast period minus baseline functional connectivity (r_0). The significance of Δr was evaluated via permutation resampling (see Statistical analyses, below).

Graph-theoretic analyses—Graph analyses were based on a set of cortical parcels (see ROI selection, above) that were assigned to the face, lower-extremity and upper-extremity somatomotor networks (SMN). We excluded any parcels that were located outside of the pre- and post-central gyri. The resulting set of ROIs for each participant are shown in Figure 3A. Functional connectivity was computed for all pairs of somatomotor parcels and then averaged across sessions to produce a weighted graph of the SMN for each experimental period (Pre, Cast, Post). Thresholded graphs (FC > 0.3) were displayed as spring-embedded

plots (Figure 3B), as previously described (Gordon et al., 2017). Next, we computed modularity (Bullmore and Sporns, 2009; Newman, 2004) for each graph. Modularity (Figure 3C) quantifies the extent to which different communities in a graph dissociate from one another. We defined two communities for computing modularity: 1) the casted upper extremity parcels (left- hemisphere parcels assigned to the upper-extremity SMN) and 2) the remainder of the SMN (bilateral lower-extremity and face SMN parcels and right-hemisphere upper-extremity SMN parcels). Thus, modularity reflects the degree of separation between the casted-extremity representation and the remainder of the SMN. Modularity (Q) is computed as:

$$Q = \frac{1}{2m} \sum_{ij} \left[A_{ij} - \frac{k_i k_j}{2m} \right] \delta(c_i, c_j) \quad (2)$$

where i and j are nodes in the graph, A_{ij} is the connection strength between nodes i and j , k_i and k_j the sums of all connection weights involving node i and node j , respectively, m is the sum of all connection weights in the graph, c_i and c_j are the community assignments of node i and node j , respectively, and δ is the Kronecker delta function (1 if c_i and c_j are identical and zero otherwise). Statistical significance of changes in modularity were evaluated using permutation resampling (see Statistical analysis, below).

Spectral analyses—rs-fMRI signals from L-SM1_{ue} and R-SM1_{ue} were Fourier transformed to obtain amplitude density spectra. Spectra from all 30-minute scans in each participant are shown in Figure 4. Amplitude of low- frequency fluctuations (Zang et al., 2007) (ALFF) for L-SM1_{ue} and R-SM1_{ue} was calculated as the root mean square of amplitude across low frequencies (0.05 – 0.1 Hz). A daily time course of L-SM1_{ue} and R-SM1_{ue} ALFF for each participant is shown in Figure 4. ALFF during the cast period was compared to ALFF during the pre period using an unpaired t-test (see Statistical Analyses, below).

Pulse detection—Example pulses were initially selected by visual inspection of L-SM1_{ue} and R-SM1_{ue} rs-fMRI signals. Based on these examples, threshold criteria were set to define pulses as large (>0.4% rs-fMRI signal change in L-SM1_{ue}), unilateral (L-SM1_{ue} minus R-SM1_{ue} > 0.3% rs-fMRI signal change) peaks in the L-SM1_{ue} rs-fMRI signal. The number of pulses detected during each 30-minute rs-fMRI scan is shown in Figure 5C. To ensure that results did not depend on specific thresholds, we repeated all analyses using a range of thresholds (L-SM1_{ue} > 0.2% to 1.2% signal change; (L-SM1_{ue} – R-SM1_{ue}) > 0.0% to 0.4% signal change). All thresholds yielded qualitatively similar results. Once pulses were detected in L-SM1_{ue}, we used an analysis of variance (Clare et al., 1999) (ANOVA) of whole-brain rs-fMRI signals surrounding each L-SM1_{ue} pulse (13.2 seconds before to 17.6 seconds after each pulse peak) to determine if other brain regions showed consistent patterns of activity during pulses. Because the ANOVA F-statistic increases with increasing sample sizes, we divided by the square root of n (the number of pulses) to normalize maps across participants. The resulting maps are shown in Figures 6 and S4.

Pulse timing analyses—The exact timing of each pulse was estimated by temporally aligning each pulse event with the mean L-SM1_{ue} pulse waveform. This alignment was implemented by parabolic optimization of the cross-correlation between each pulse event in each region of interest (L-SM1_{ue}, L-SMA_{ue}, and R-Cblm_{ue}) and the mean pulse waveform. A similar approach was recently shown to provide reliable estimates of sub-TR time delays between rs-fMRI time series (Raut et al., 2019). Figures 6C and S4 show the relative time delays of pulse waveforms extracted from L-SM1_{ue}, L-SMA_{ue}, and R-Cblm_{ue}. Pulse times between regions were then compared using Wilcoxon signed rank tests (see Statistical analyses, below).

Hand movement analyses—Pressure readings were acquired at 400 Hz. Pressure traces were low-pass filtered (<2 Hz) to remove high-frequency noise and differentiated to remove occasional shifts in baseline. The amplitude of pressure traces was normalized across recordings by dividing by the median deviation from the mean. Fully processed traces from the pressure bladder during 30-minute rs-fMRI scans are shown in Figure S5. Movements were detected by squaring the processed pressure trace, smoothing with a kernel of 1 second, and applying a threshold of 0.6. Disuse pulses detected in the rs-fMRI signals (see Pulse detection, above) were classified as spontaneous if no movements were detected within 8 seconds preceding the pulse peak. The percentage of pulses classified as spontaneous during each session is shown in Figure S5.

Statistical analyses—All statistical tests were performed identically for each participant. Whenever appropriate, we used simple parametric statistical tests:

- Accelerometry use counts measured during each day of the cast period (Nico: n = 13 days; Ashley: n = 14; Omar: n = 14) were compared to use counts during the pre period (Nico: n = 7; Ashley: n = 14; Omar: n = 14) using a two-sided, unpaired t-test (Nico: d.f. = 18; Ashley: d.f. = 26; Omar: d.f. = 26). This test was performed separately for each upper extremity (Figure S1).
- Grip strength immediately after cast removal, measured in triplicate for each hand (all participants: n = 3 measurements), was compared to all strength measurements acquired prior to casting (Nico: n=3; Ashley: n=6; Omar: n=42) using a two-sided, un-paired t-test (Nico: d.f. = 4, Ashley: d.f. = 7, Omar: d.f. = 43). This test was performed separately for each upper extremity (Figure 1D)
- Performance on the Purdue pegboard task (# pegs inserted in 30 seconds) immediately after cast removal (all participants: n = 3 trials), was compared to all trials conducted prior to casting (Nico: n=3; Ashley: n=6; Omar: n=9) using a two-sided, un-paired t-test (Nico: d.f. = 4, Ashley: d.f. = 7, Omar: d.f. = 10). This test was performed separately for each upper extremity (Figure S1)
- To determine how quickly functional connectivity (FC) between the left and right somatomotor cortex (L-SM1_{ue} and R-SM1_{ue}) became significantly decreased in each participant, FC measured during each session of the cast period was compared to all sessions of the pre period (Nico: n = 10 sessions; Ashley: n = 12; Omar: n = 14) using two-sided, one-sample t- tests (Nico: d.f. = 9; Ashley: d.f. =

11; Omar: d.f. = 13) conducted separately for each Cast session. We reported the time required for FC during a Cast session to become significantly lower ($P < 0.05$) than FC during the pre period

- Amplitude of low frequency fluctuations (ALFF) in $L-SM1_{ue}$ measured during each session of the cast period (Nico: $n = 13$ sessions; Ashley: $n = 13$; Omar: $n = 14$) was compared to ALFF measured during each session of the pre period (Nico: $n = 10$; Ashley: $n = 12$; Omar: $n = 14$) using a two-sided, unpaired t-test (Nico: d.f. = 21, Ashley: d.f. = 23, Omar: d.f. = 26). This test was repeated for $R-SM1_{ue}$, $L-SM1_{le}$, and $L-SM1_{face}$ (Figure 4)
- The number of disuse pulses detected in $L-SM1_{ue}$ during each session of the cast period (Nico: $n = 13$ sessions; Ashley: $n = 13$; Omar: $n = 14$) was compared to the number of pulses detected during each session of the pre period (Nico: $n = 10$; Ashley: $n = 12$; Omar: $n = 14$) using a two-sided, unpaired t-test (Nico: d.f. = 21, Ashley: d.f. = 23, Omar: d.f. = 26).
- The relative timing of disuse pulses in $L-SMA_{ue}$ and $L-SM1_{ue}$ was compared using a Wilcoxon signed rank test (Nico: d.f. = 64, Ashley: d.f. = 143, Omar: d.f. = 156). This test was repeated to compare the relative timing of disuse pulses in $L-SMA_{ue}$ and $R-Cblm_{ue}$ and the relative timing of disuse pulses in $L-SM1_{ue}$ and $R-Cblm_{ue}$ (Figures 6C and S4).
- To evaluate the effects of wearing a removable cast during scanning, FC between $L-SM1_{ue}:R-SM1_{ue}$ and $L-Cblm_{ue}:R-Cblm_{ue}$ measured while participants wore removable casts (“On” sessions; Nico: $n = 6$ sessions; Ashley: $n = 12$; Omar: $n = 6$) was compared to sessions acquired without casts (“Off” sessions; Nico: $n = 6$ sessions; Ashley: $n = 12$; Omar: $n = 6$) using a two-sided un-paired t-test (Nico: d.f. = 10; Ashley: d.f. = 22; Omar: d.f. = 10). The same test was used to compare the number of pulse-like events detected during On sessions to the number of events detected in Off sessions (Figure S6).

When parametric statistical tests were not appropriate to test a specific hypothesis, we tested results against a null distribution generated via permutation resampling. In each case, our null hypothesis was that no changes occurred due to casting and any observed differences were due to measurement error. We modeled this null hypothesis by permuting the order of MRI sessions 10,000 times, eliminating any temporal relationship between sessions and the casting intervention. Each permuted sample was treated exactly as the actual data in order to compute a null distribution for the value of interest. The P-value reported for each test represents the two-sided probability that a value in the null distribution has a greater magnitude than the observed value. Permutation resampling was used to generate null distributions for the following values:

- Change in functional connectivity (r) during casting, based on the exponential decay model (Figures 2B-D and S2)
- Change in modularity of the somatomotor network (Q) during casting (Figure 3)

All analyses were hypothesis driven and tested in a small number of regions of interest (ROIs), defined using independent data (task activations or baseline FC gradients). Correction for multiple comparisons was not necessary for most analyses. In cases where tests were applied to multiple ROIs, a Benjamini-Hochberg procedure was applied to correct for multiple comparisons, maintaining false discovery rates < 0.05 . This correction was applied to the following tests:

- Decreases in homotopic FC, tested in three pairs of ROIs: L-SM1_{ue}:R-SM1_{ue}, R-Cblm_{ue}:L-Cblm_{ue}, and L-SMA_{ue}:R-SMA_{ue} (Figures 2 and S2)
- Delays in pulse timing, tested between three pairs of ROIs: L-SM1_{ue}→R-Cblm_{ue}, L-SMA_{ue}→L-SM1_{ue}, and L-SMA_{ue}→R-Cblm_{ue} (Figures 6C and S4)

Each of the three participants constituted a separate replication of the experiment, rather than multiple comparisons, so no correction was necessary for tests repeated in each participant.

Data visualization—Regions of interest and whole-brain pulse maps were shown on cortical surfaces generated by FreeSurfer (Fischl, 2012) and Human Connectome Project (HCP) Workbench software packages (Marcus et al., 2011). These images were rendered using HCP Workbench (Marcus et al., 2011). All other figures were produced using Matlab (www.mathworks.com).

Supplementary Material

Refer to Web version on PubMed Central for supplementary material.

Acknowledgements:

We thank Deanna M. Barch and Jin-Moo Lee for their comments on this research and Scott Gericke for help with the visual presentation of the results. This work was supported by NIH grants F31NS110332 (D.J.N.), NS088590 (N.U.F.D.), TR000448 (N.U.F.D.), MH1000872 (T.O.L.), 1R25MH112473 (T.O.L.), 5T32 MH100019-02 (S.M.), MH104592 (D.J.G.), 1P30NS098577 (to the Neuroimaging Informatics and Analysis Center); the US Department of Veterans Affairs Clinical Sciences Research and Development Service grant 11K2CX001680 (E.M.G.); Kiwanis Neuroscience Research Foundation (N.U.F.D. and B.L.S.); the Jacobs Foundation grant 2016121703 (N.U.F.D.); the Child Neurology Foundation (N.U.F.D.); the McDonnell Center for Systems Neuroscience (N.U.F.D. and B.L.S.); the Mallinckrodt Institute of Radiology grant 14-011 (N.U.F.D.); the Hope Center for Neurological Disorders (N.U.F.D., B.L.S., and S.E.P.). The views expressed in this article are those of the authors and do not necessarily reflect the position or policy of the Department of Veterans Affairs or the U.S. government.

REFERENCES

- Ackman JB, Burbridge TJ, and Crair MC (2012). Retinal waves coordinate patterned activity throughout the developing visual system. *Nature* 490, 219–225. [PubMed: 23060192]
- Barch DM, Burgess GC, Harms MP, Petersen SE, Schlaggar BL, Corbetta M, Glasser MF, Curtiss S, Dixit S, Feldt C, et al. (2013). Function in the human connectome: task-fMRI and individual differences in behavior. *Neuroimage* 80, 169–189. [PubMed: 23684877]
- Behzadi Y, Restom K, Liao J, and Liu TT (2007). A component based noise correction method (CompCor) for BOLD and perfusion based fMRI. *Neuroimage* 37, 90–101. [PubMed: 17560126]
- Biswal B, Yetkin FZ, Haughton VM, and Hyde JS (1995). Functional connectivity in the motor cortex of resting human brain using echo-planar MRI. *Magn Reson Med* 34, 537–541. [PubMed: 8524021]
- Bullmore E, and Sporns O (2009). Complex brain networks: graph theoretical analysis of structural and functional systems. *Nat Rev Neurosci* 10, 186–198. [PubMed: 19190637]

- Buzsáki G (2015). Hippocampal sharp wave-ripple: A cognitive biomarker for episodic memory and planning. *Hippocampus* 25, 1073–1188. [PubMed: 26135716]
- Buzsáki G (2019). *The brain from inside out*. (New York, NY: Oxford University Press).
- Carter AR, Patel KR, Astafiev SV, Snyder AZ, Rengachary J, Strube MJ, Pope A, Shimony JS, Lang CE, Shulman GL, and Corbetta M (2012). Upstream dysfunction of somatomotor functional connectivity after corticospinal damage in stroke. *Neurorehabil Neural Repair* 26, 7–19. [PubMed: 21803932]
- Clare S, Humberstone M, Hykin J, Blumhardt LD, Bowtell R, and Morris P (1999). Detecting activations in event-related fMRI using analysis of variance. *Magn Reson Med* 42, 1117–1122. [PubMed: 10571933]
- Dosenbach NU, Fair DA, Cohen AL, Schlaggar BL, and Petersen SE (2008). A dual-networks architecture of top-down control. *Trends Cogn Sci* 12, 99–105. [PubMed: 18262825]
- Dosenbach NU, Nardos B, Cohen AL, Fair DA, Power JD, Church JA, Nelson SM, Wig GS, Vogel AC, Lessov-Schlaggar CN, et al. (2010). Prediction of individual brain maturity using fMRI. *Science* 329, 1358–1361. [PubMed: 20829489]
- Dosenbach NUF, Koller JM, Earl EA, Miranda-Dominguez O, Klein RL, Van AN, Snyder AZ, Nagel BJ, Nigg JT, Nguyen AL, et al. (2017). Real-time motion analytics during brain MRI improve data quality and reduce costs. *Neuroimage* 161, 80–93. [PubMed: 28803940]
- Fair DA, Miranda-Dominguez O, Snyder AZ, Perrone A, Earl EA, Van AN, Koller JM, Feczko E, Tisdall MD, van der Kouwe A, et al. (2020). Correction of respiratory artifacts in MRI head motion estimates. *Neuroimage* 208, 116400.
- Fischl B (2012). FreeSurfer. *Neuroimage* 62, 774–781. [PubMed: 22248573]
- Gainey MA, Aman JW, and Feldman DE (2018). Rapid Disinhibition by Adjustment of PV Intrinsic Excitability during Whisker Map Plasticity in Mouse S1. *J Neurosci* 38, 4749–4761. [PubMed: 29678876]
- Gordon EM, Laumann TO, Gilmore AW, Newbold DJ, Greene DJ, Berg JJ, Ortega M, Hoyt-Drazen C, Gratton C, Sun H, et al. (2017). Precision Functional Mapping of Individual Human Brains. *Neuron* 95, 791–807 e797. [PubMed: 28757305]
- Gratton C, Koller JM, Shannon W, Greene DJ, Maiti B, Snyder AZ, Petersen SE, Perlmutter JS, and Campbell MC (2019). Emergent Functional Network Effects in Parkinson Disease. *Cereb Cortex* 29, 2509–2523. [PubMed: 29878081]
- Gratton C, Laumann TO, Nielsen AN, Greene DJ, Gordon EM, Gilmore AW, Nelson SM, Coalson RS, Snyder AZ, Schlaggar BL, et al. (2018). Functional Brain Networks Are Dominated by Stable Group and Individual Factors, Not Cognitive or Daily Variation. *Neuron* 98, 439–452 e435. [PubMed: 29673485]
- Grayson DS, Bliss-Moreau E, Machado CJ, Bennett J, Shen K, Grant KA, Fair DA, and Amaral DG (2016). The Rhesus Monkey Connectome Predicts Disrupted Functional Networks Resulting from Pharmacogenetic Inactivation of the Amygdala. *Neuron* 91, 453–466. [PubMed: 27477019]
- Grayson DS, and Fair DA (2017). Development of large-scale functional networks from birth to adulthood: A guide to the neuroimaging literature. *Neuroimage* 160, 15–31. [PubMed: 28161313]
- Greene DJ, Marek S, Gordon EM, Siegel JS, Gratton C, Laumann TO, Gilmore AW, Berg JJ, Nguyen AL, Dierker D, et al. (2020). Integrative and Network-Specific Connectivity of the Basal Ganglia and Thalamus Defined in Individuals. *Neuron* 105, 742–758 e746. [PubMed: 31836321]
- Guerra-Carrillo B, Mackey AP, and Bunge SA (2014). Resting-state fMRI: a window into human brain plasticity. *Neuroscientist* 20, 522–533. [PubMed: 24561514]
- Harmelech T, and Malach R (2013). Neurocognitive biases and the patterns of spontaneous correlations in the human cortex. *Trends Cogn Sci* 17, 606–615. [PubMed: 24182697]
- Hoyt CR, Van AN, Ortega M, Koller JM, Everett EA, Nguyen AL, Lang CE, Schlaggar BL, and Dosenbach NUF (2019). Detection of Pediatric Upper Extremity Motor Activity and Deficits With Accelerometry. *JAMA Netw Open* 2, e192970.
- Jenkinson M, Beckmann CF, Behrens TE, Woolrich MW, and Smith SM (2012). Fsl. *Neuroimage* 62, 782–790. [PubMed: 21979382]
- Katz LC, and Shatz CJ (1996). Synaptic activity and the construction of cortical circuits. *Science* 274, 1133–1138. [PubMed: 8895456]

- Khazipov R, Sirota A, Leinekugel X, Holmes GL, Ben-Ari Y, and Buzsaki G (2004). Early motor activity drives spindle bursts in the developing somatosensory cortex. *Nature* 432, 758–761. [PubMed: 15592414]
- Klinzing JG, Niethard N, and Born J (2019). Mechanisms of systems memory consolidation during sleep. *Nat Neurosci* 22, 1598–1610. [PubMed: 31451802]
- Kraft AW, Mitra A, Bauer AQ, Snyder AZ, Raichle ME, Culver JP, and Lee JM (2017). Visual experience sculpts whole-cortex spontaneous infraslow activity patterns through an Arc-dependent mechanism. *Proc Natl Acad Sci U S A* 114, E9952–E9961. [PubMed: 29087327]
- Lancaster J, Glass TG, Lankipalli BR, Downs H, Mayberg H, and Fox PT (1995). A modality-independent approach to spatial normalization of tomographic images of the human brain. *Hum Brain Mapp* 3, 209–223.
- Laumann TO, Gordon EM, Adeyemo B, Snyder AZ, Joo SJ, Chen MY, Gilmore AW, McDermott KB, Nelson SM, Dosenbach NU, et al. (2015). Functional System and Areal Organization of a Highly Sampled Individual Human Brain. *Neuron* 87, 657–670. [PubMed: 26212711]
- Laumann TO, Snyder AZ, Mitra A, Gordon EM, Gratton C, Adeyemo B, Gilmore AW, Nelson SM, Berg JJ, Greene DJ, et al. (2017). On the Stability of BOLD fMRI Correlations. *Cereb Cortex* 27, 4719–4732. [PubMed: 27591147]
- Lewis CM, Baldassarre A, Committeri G, Romani GL, and Corbetta M (2009). Learning sculpts the spontaneous activity of the resting human brain. *Proc Natl Acad Sci U S A* 106, 17558–17563. [PubMed: 19805061]
- Liepert J, Storch P, Fritsch A, and Weiller C (2000). Motor cortex disinhibition in acute stroke. *Clin Neurophysiol* 111, 671–676. [PubMed: 10727918]
- Lindquist MA, Meng Loh J, Atlas LY, and Wager TD (2009). Modeling the hemodynamic response function in fMRI: efficiency, bias and mis-modeling. *Neuroimage* 45, S187–198. [PubMed: 19084070]
- Makin TR, Scholz J, Filippini N, Henderson Slater D, Tracey I, and Johansen-Berg H (2013). Phantom pain is associated with preserved structure and function in the former hand area. *Nat Commun* 4, 1570. [PubMed: 23463013]
- Marcus DS, Harwell J, Olsen T, Hodge M, Glasser MF, Prior F, Jenkinson M, Laumann T, Curtiss SW, and Van Essen DC (2011). Informatics and data mining tools and strategies for the human connectome project. *Front Neuroinform* 5, 4. [PubMed: 21743807]
- Marek S, Siegel JS, Gordon EM, Raut RV, Gratton C, Newbold DJ, Ortega M, Laumann TO, Adeyemo B, Miller DB, et al. (2018). Spatial and Temporal Organization of the Individual Human Cerebellum. *Neuron* 100, 977–993 e977. [PubMed: 30473014]
- Merzenich MM, Kaas JH, Wall J, Nelson RJ, Sur M, and Felleman D (1983). Topographic reorganization of somatosensory cortical areas 3b and 1 in adult monkeys following restricted deafferentation. *Neuroscience* 8, 33–55. [PubMed: 6835522]
- Milliken GW, Plautz EJ, and Nudo RJ (2013). Distal forelimb representations in primary motor cortex are redistributed after forelimb restriction: a longitudinal study in adult squirrel monkeys. *J Neurophysiol* 109, 1268–1282. [PubMed: 23236004]
- Mitra A, Snyder AZ, Hacker CD, and Raichle ME (2014). Lag structure in resting-state fMRI. *J Neurophysiol* 111, 2374–2391. [PubMed: 24598530]
- Murphy TH, and Corbett D (2009). Plasticity during stroke recovery: from synapse to behaviour. *Nat Rev Neurosci* 10, 861–872. [PubMed: 19888284]
- Newman ME (2004). Analysis of weighted networks. *Phys Rev E Stat Nonlin Soft Matter Phys* 70, 056131.
- Nielsen AN, Gratton C, Church JA, Dosenbach NUF, Black KJ, Petersen SE, Schlaggar BL, and Greene DJ (2020). Atypical Functional Connectivity in Tourette Syndrome Differs Between Children and Adults. *Biol Psychiatry* 87, 164–173. [PubMed: 31472979]
- Nielsen AN, Greene DJ, Gratton C, Dosenbach NUF, Petersen SE, and Schlaggar BL (2019). Evaluating the Prediction of Brain Maturity From Functional Connectivity After Motion Artifact Denoising. *Cereb Cortex* 29, 2455–2469. [PubMed: 29850877]
- Oldfield RC (1971). The assessment and analysis of handedness: the Edinburgh inventory. *Neuropsychologia* 9, 97–113. [PubMed: 5146491]

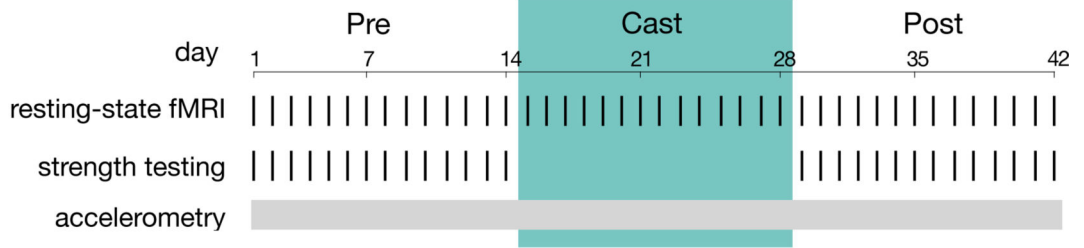
- Pawela CP, Biswal BB, Hudetz AG, Li R, Jones SR, Cho YR, Matloub HS, and Hyde JS (2010). Interhemispheric neuroplasticity following limb deafferentation detected by resting-state functional connectivity magnetic resonance imaging (fcMRI) and functional magnetic resonance imaging (fMRI). *Neuroimage* 49, 2467–2478. [PubMed: 19796693]
- Power JD (2017). A simple but useful way to assess fMRI scan qualities. *Neuroimage* 154, 150–158. [PubMed: 27510328]
- Power JD, Barnes KA, Snyder AZ, Schlaggar BL, and Petersen SE (2012). Spurious but systematic correlations in functional connectivity MRI networks arise from subject motion. *Neuroimage* 59, 2142–2154. [PubMed: 22019881]
- Power JD, Cohen AL, Nelson SM, Wig GS, Barnes KA, Church JA, Vogel AC, Laumann TO, Miezin FM, Schlaggar BL, and Petersen SE (2011). Functional network organization of the human brain. *Neuron* 72, 665–678. [PubMed: 22099467]
- Raichle ME (2006). Neuroscience. The brain's dark energy. *Science* 314, 1249–1250. [PubMed: 17124311]
- Raut RV, Mitra A, Marek S, Ortega M, Snyder AZ, Tanenbaum A, Laumann TO, Dosenbach NUF, and Raichle ME (2020). Organization of Propagated Intrinsic Brain Activity in Individual Humans. *Cereb Cortex* 30, 1716–1734. [PubMed: 31504262]
- Raut RV, Mitra A, Snyder AZ, and Raichle ME (2019). On time delay estimation and sampling error in resting-state fMRI. *Neuroimage* 194, 211–227. [PubMed: 30902641]
- Reynolds JN, Hyland BI, and Wickens JR (2001). A cellular mechanism of reward-related learning. *Nature* 413, 67–70. [PubMed: 11544526]
- Rosenthal ZP, Raut RV, Yan P, Koko D, Kraft AW, Czerniewski L, Acland B, Mitra A, Snyder LH, Bauer AQ, et al. (2020). Local perturbations of cortical excitability propagate differentially through large-scale functional networks. *Cereb Cortex* 30, 3352–3369. [PubMed: 32043145]
- Rosvall M, and Bergstrom CT (2008). Maps of random walks on complex networks reveal community structure. *Proc Natl Acad Sci U S A* 105, 1118–1123. [PubMed: 18216267]
- Shannon BJ, Dosenbach RA, Su Y, Vlassenko AG, Larson-Prior LJ, Nolan TS, Snyder AZ, and Raichle ME (2013). Morning-evening variation in human brain metabolism and memory circuits. *J Neurophysiol* 109, 1444–1456. [PubMed: 23197455]
- Shannon BJ, Vaishnavi SN, Vlassenko AG, Shimony JS, Rutlin J, and Raichle ME (2016). Brain aerobic glycolysis and motor adaptation learning. *Proc Natl Acad Sci U S A* 113, E3782–3791. [PubMed: 27217563]
- Siegel JS, Seitzman BA, Ramsey LE, Ortega M, Gordon EM, Dosenbach NUF, Petersen SE, Shulman GL, and Corbetta M (2018). Re-emergence of modular brain networks in stroke recovery. *Cortex* 101, 44–59. [PubMed: 29414460]
- Smyser CD, Inder TE, Shimony JS, Hill JE, Degnan AJ, Snyder AZ, and Neil JJ (2010). Longitudinal analysis of neural network development in preterm infants. *Cereb Cortex* 20, 2852–2862. [PubMed: 20237243]
- Sylvester CM, Yu Q, Srivastava AB, Marek S, Zheng A, Alexopoulos D, Smyser CD, Shimony JS, Ortega M, Dierker DL, et al. (2020). Individual-specific functional connectivity of the amygdala: A substrate for precision psychiatry. *Proc Natl Acad Sci U S A* 117, 3808–3818. [PubMed: 32015137]
- Talairach J, and Tournoux P (1988). *Co-planar stereotaxic atlas of the human brain : 3-dimensional proportional system: an approach to cerebral imaging* (Stuttgart; New York: Georg Thieme).
- Tiffin J, and Asher EJ (1948). The Purdue pegboard; norms and studies of reliability and validity. *J Appl Psychol* 32, 234–247. [PubMed: 18867059]
- Tolonen M, Palva JM, Andersson S, and Vanhatalo S (2007). Development of the spontaneous activity transients and ongoing cortical activity in human preterm babies. *Neuroscience* 145, 997–1006. [PubMed: 17307296]
- Toyoizumi T, Miyamoto H, Yazaki-Sugiyama Y, Atapour N, Hensch TK, and Miller KD (2013). A theory of the transition to critical period plasticity: inhibition selectively suppresses spontaneous activity. *Neuron* 80, 51–63. [PubMed: 24094102]

- van der Pas SC, Verbunt JA, Breukelaar DE, van Woerden R, and Seelen HA (2011). Assessment of arm activity using triaxial accelerometry in patients with a stroke. *Arch Phys Med Rehabil* 92, 1437–1442. [PubMed: 21878214]
- Wellman CL, Arnold LL, Garman EE, and Garraghty PE (2002). Acute reductions in GABAA receptor binding in layer IV of adult primate somatosensory cortex after peripheral nerve injury. *Brain Res* 954, 68–72. [PubMed: 12393234]
- Wenger E, Kuhn S, Verrel J, Martensson J, Bodammer NC, Lindenberger U, and Lovden M (2017). Repeated Structural Imaging Reveals Nonlinear Progression of Experience-Dependent Volume Changes in Human Motor Cortex. *Cereb Cortex* 27, 2911–2925. [PubMed: 27226440]
- Wiesel TN, and Hubel DH (1965). Comparison of the effects of unilateral and bilateral eye closure on cortical unit responses in kittens. *J Neurophysiol* 28, 1029–1040. [PubMed: 5883730]
- Yeo BT, Krienen FM, Sepulcre J, Sabuncu MR, Lashkari D, Hollinshead M, Roffman JL, Smoller JW, Zollei L, Polimeni JR, et al. (2011). The organization of the human cerebral cortex estimated by intrinsic functional connectivity. *J Neurophysiol* 106, 1125–1165. [PubMed: 21653723]
- Zang YF, He Y, Zhu CZ, Cao QJ, Sui MQ, Liang M, Tian LX, Jiang TZ, and Wang YF (2007). Altered baseline brain activity in children with ADHD revealed by resting-state functional MRI. *Brain Dev* 29, 83–91. [PubMed: 16919409]
- Zhang Y, Brady M, and Smith S (2001). Segmentation of brain MR images through a hidden Markov random field model and the expectation-maximization algorithm. *IEEE Trans Med Imaging* 20, 45–57. [PubMed: 11293691]

Highlights

- Casting the dominant upper extremity for two weeks caused disuse and weakness
- Disused brain circuits functionally disconnected from the rest of the motor system
- Connectivity within disused circuits was maintained throughout casting
- Disuse-driven spontaneous activity pulses propagated through disused circuits

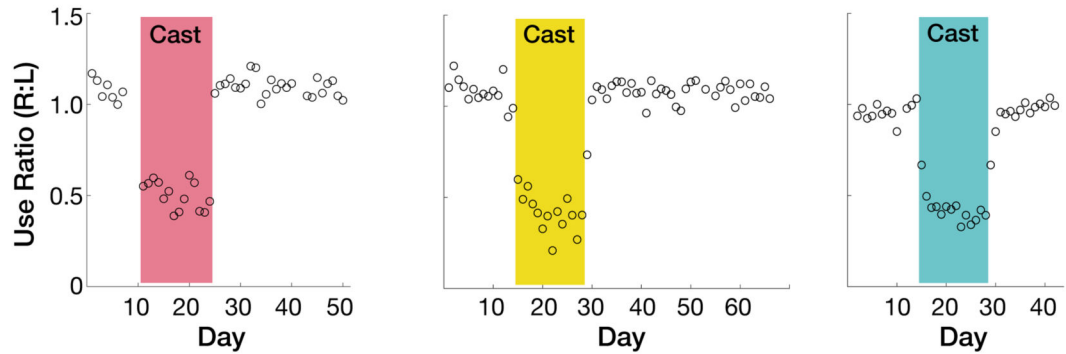
A Experimental design



B Casts



C Accelerometry



D Strength testing

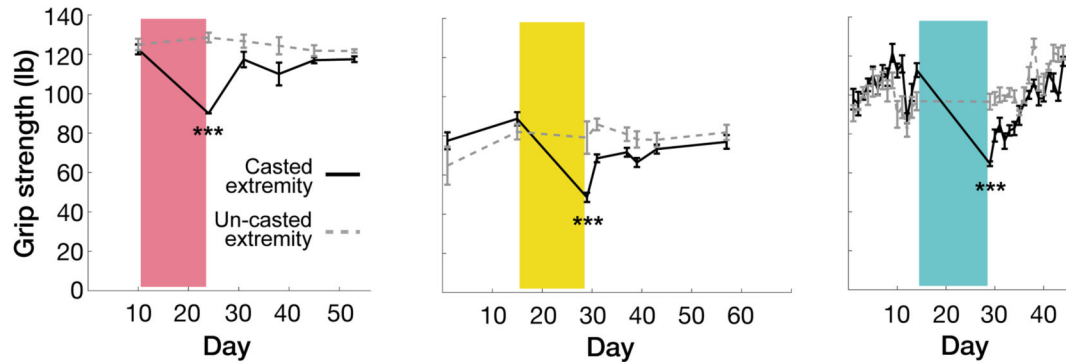
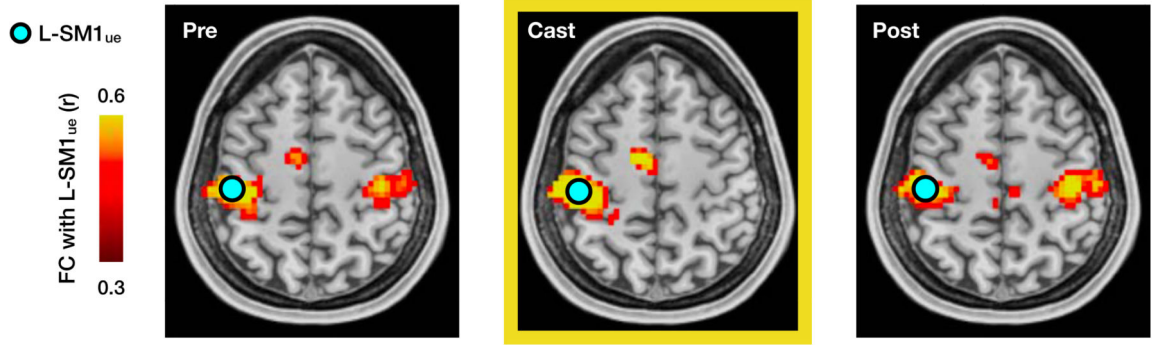
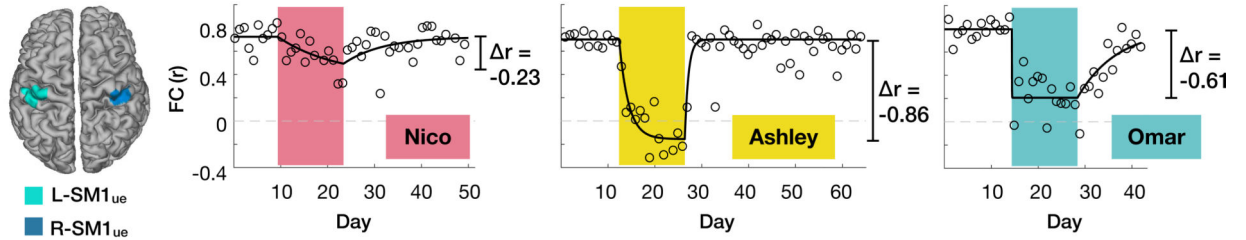


Figure 1. Casting caused disuse and reduced strength of the dominant upper extremity. (A) Experimental design for an example participant (Omar; all participants Figure S1). (B) Casts covered the entire dominant upper extremity. Cast colors are used in subsequent figures to identify participants: pink (Nico), yellow (Ashley), green (Omar). (C) Daily accelerometry data from both wrists, plotted as use ratios (R/L use counts). Use count = seconds each day when RMS acceleration > 0.16 m/s². Daily use counts for each wrist shown in Figure S1. (D) Grip strength before and after casting (***)P < 0.001). Error bars indicate s.e.m. across three repeated measurements.

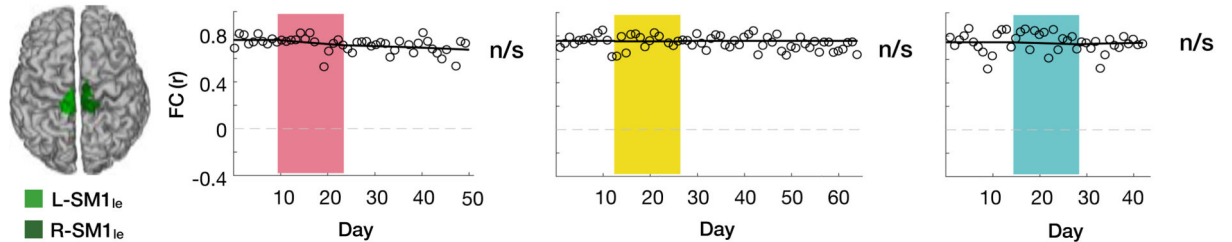
A Functional connectivity (FC) seed maps



B Daily time course of FC: upper extremity



C Daily time course of FC: lower extremity (negative control)



D Daily time course of FC: face (negative control)

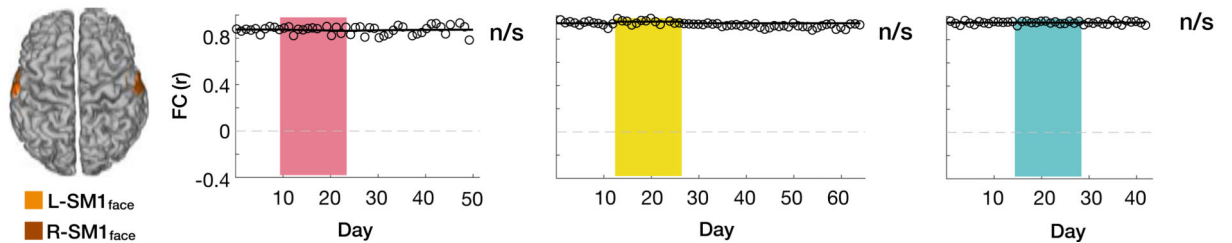


Figure 2. Disused somatomotor cortex became functionally uncoupled from opposite hemisphere.

(A) Seed maps showing functional connectivity (FC) of each voxel with the left primary somatomotor cortex (L-SM1_{ue}) during scans acquired before, during and after casting (Pre, Cast, Post) in an example participant (Ashley). The L-SM1_{ue} region of interest (ROI) was defined using task functional MRI. (B) Daily time course of FC between L-SM1_{ue} and R-SM1_{ue} for each participant. r values are based on a time-varying exponential decay model (black lines, $dr/dt = \alpha(r_{\infty} - r)$; Nico: $P = 0.002$, Ashley: $P < 0.001$, Omar: $P < 0.001$). (C and

D) Daily time course of FC in lower extremity (C) and face (D) regions of the left and right somatomotor cortex.

Author Manuscript

Author Manuscript

Author Manuscript

Author Manuscript

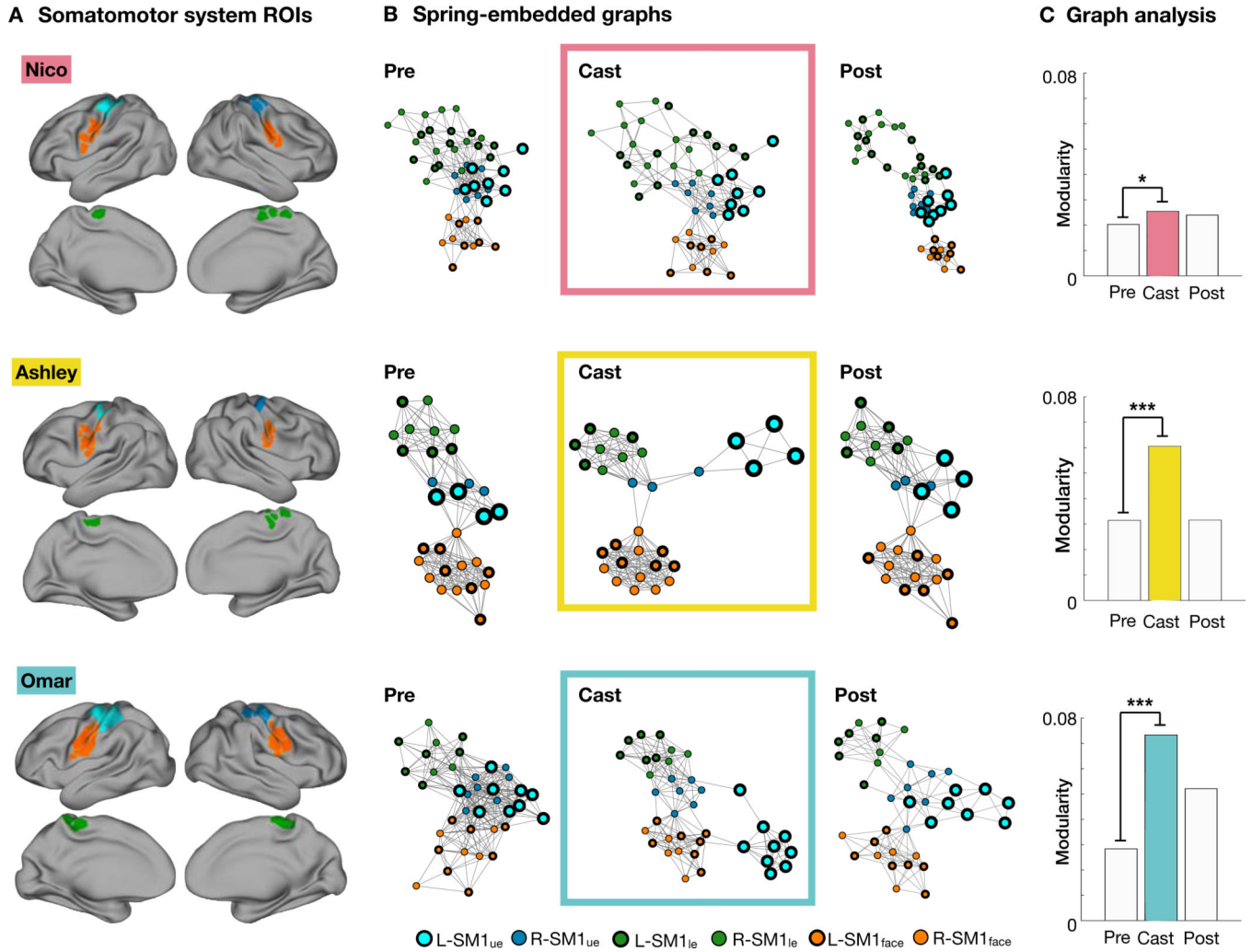
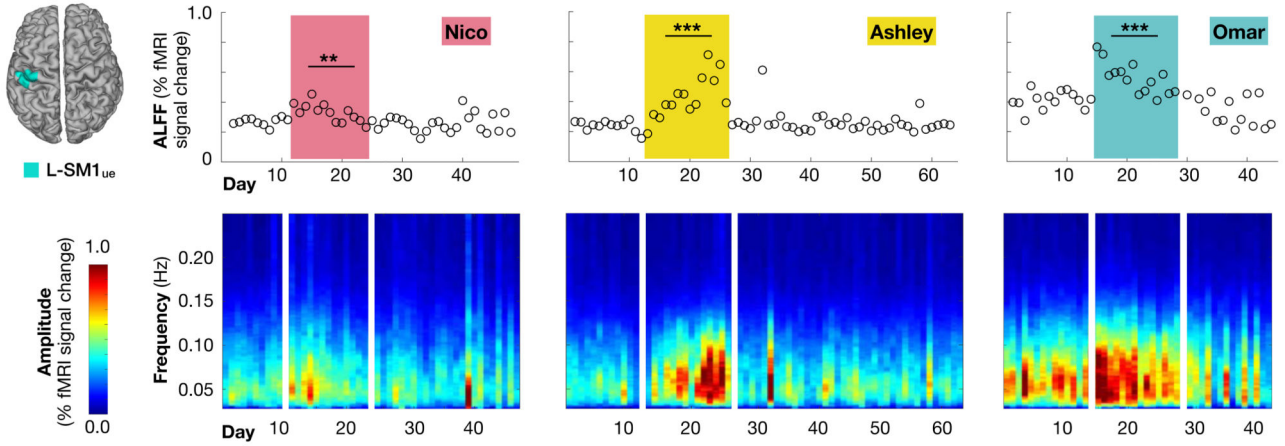


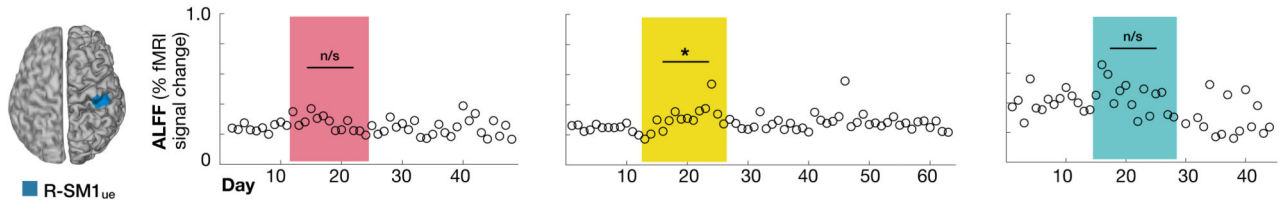
Figure 3. Disused somatomotor cortex dissociated from the remainder of the somatomotor system.

(A) Regions of interest (ROIs) in the lower extremity (green), upper extremity (cyan/blue) and face (orange) subdivisions of the somatomotor system for each participant. ROIs were selected using a functional connectivity gradient-based approach (Gordon et al., 2017). (B) Spring-embedded graph representation of the somatomotor system before, during and after casting. The disused region (L-SM1_{ue}) separated from the remainder of the somatomotor cortex during the cast period but remained internally connected. (C) Modularity quantifies the degree of dissociation between L-SM1_{ue} and the rest of the somatomotor cortex. All participants showed increased modularity during the cast period. *P < 0.05; ***P < 0.001.

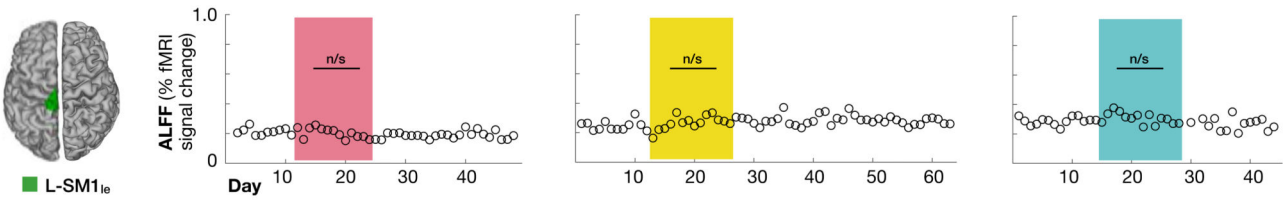
A L-SM1_{ue} amplitude



B R-SM1_{ue} amplitude



C L-SM1_{le} amplitude (negative control)



D L-SM1_{face} amplitude (negative control)

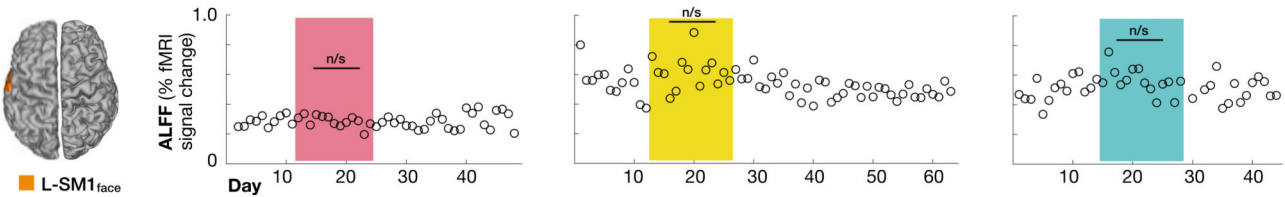


Figure 4. Disused somatomotor cortex (L-SM1_{ue}) showed increased amplitude of low- frequency fluctuations (ALFF).

(A) *Top*: ALFF in resting-state functional MRI (rs-fMRI) signals recorded from L-SM1_{ue} on each day of the experiment. All participants showed significantly increased L-SM1_{ue} ALFF during the cast period, relative to the pre period (Nico: +22%, $P < 0.01$; Ashley: +81%, $P < 0.001$; Omar: +36%, $P < 0.001$). *Bottom*: Amplitude spectra of L-SM1_{ue} rs-fMRI signals. (B) ALFF in R-SM1_{ue}. Only participant Ashley showed significantly increased R-SM1_{ue} ALFF during the cast period. (C) ALFF in lower-extremity somatomotor cortex (L-SM1_{le}; negative control). No participants showed significant changes during the cast period. (D)

ALFF in face somatomotor cortex (L-SM1_{face}; negative control). No participants showed significant changes during the cast period.

Author Manuscript

Author Manuscript

Author Manuscript

Author Manuscript

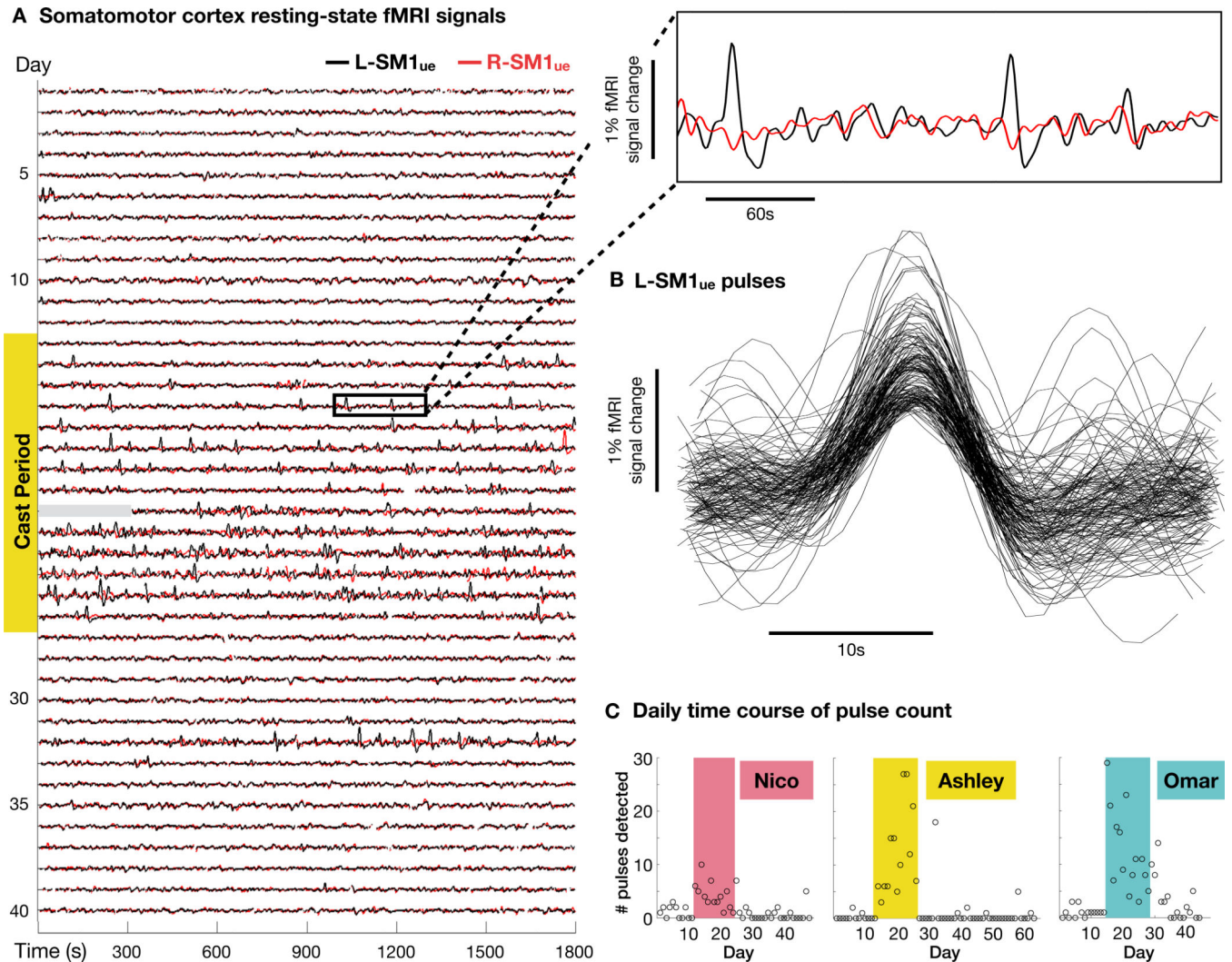
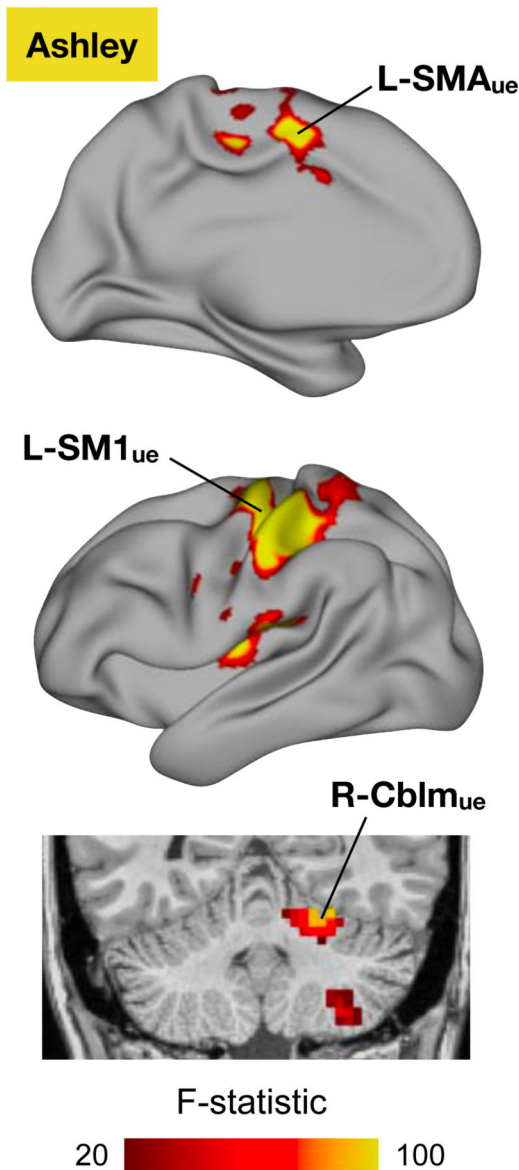
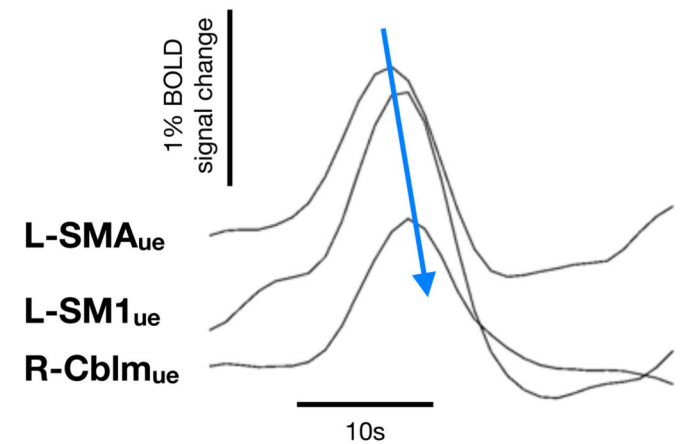
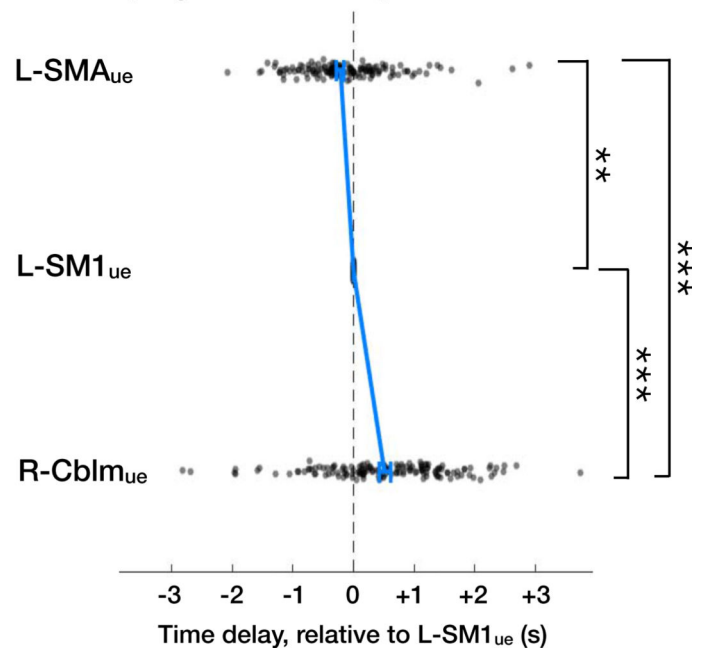


Figure 5. Disuse pulses in somatomotor cortex.

(A) Resting-state functional MRI (rs-fMRI) signals from left and right primary somatomotor cortex (L-SM1_{ue} and R-SM1_{ue}) before, during and after casting in an example participant (Ashley; all participants Figure S3). During the cast period, large pulses occur in L-SM1_{ue} (see inset at top-right). Data for first five minutes of scan 21 are unavailable (gray bar). (B) Recordings of 144 disuse pulses detected in an example participant (Ashley). (C) Number of pulses detected during each day of the experiment. All participants showed significantly more pulses per session during the cast period than during the pre period. (Nico: $P = 0.002$; Ashley: $P < 0.001$; Omar: $P < 0.001$)

A Whole-brain pulse map**B Propagation between regions****C Propagation of all pulses****Figure 6. Disuse pulses propagate through the disused somatomotor sub-circuit.**

(A) Whole-brain analysis of variance (ANOVA) of disuse pulses in an example participant (Ashley; all participants shown in Figure S4). In addition to L-SM1_{ue}, pulses also occur in left supplementary motor area (L-SMA_{ue}) and right cerebellum (R-Cblm_{ue}). (B) Example pulse in L-SMA_{ue}, L-SM1_{ue} and R-Cblm_{ue}. Note the temporal offset of peaks in each region. (C) Time delays (relative to L-SM1_{ue}) of all pulses in each region for an example participant (Ashley; all participant Figure S4). Blue lines indicate median delay \pm s.e.m. in each region. Pulses occurred first in L-SMA_{ue}, then L-SM1_{ue}, and finally in R-Cblm_{ue}. Pulse times were determined by parabolic interpolation of cross-correlations with the mean pulse time series. ** $P < 0.01$. *** $P < 0.001$.

KEY RESOURCES TABLE

REAGENT or RESOURCE	SOURCE	IDENTIFIER
Raw and processed MRI data	This manuscript	https://openneuro.org/datasets/ds1002766
MATLAB	MathWorks	RRID: SCR_001622; https://www.mathworks.com/
Connectome Workbench	(Marcus et al., 2011)	RRID: SCR_008750; https://www.humanconnectome.org/software/connectome-workbench
Freesurfer	(Fischl, 2012)	RRID: SCR_001847; https://surfer.nmr.mgh.harvard.edu/
4dfp tools	N/A	ftp://imaging.wustl.edu/pub/raichlab/4dfp_tools/
Analysis code	This manuscript	https://gitlab.com/DosenbachGreene/cast-induced-plasticity

Author Manuscript

Author Manuscript

Author Manuscript

Author Manuscript